The Astronomical Journal, 171:101 (10pp), 2026 February https://doi.org/10.3847/1538-3881/ae2d1c

Characterization of an Optical Transfer Function–based Phasing Technique for India's Large Segmented Mirror Telescope

Radhika Dharmadhikari[1,2] and Padmakar Parihar[1]
[1] Indian Institute of Astrophysics, II Block Kormangala, Bangalore, India
[2] Department of Applied Optics and Photonics, University of Calcutta, Kolkata, India
Received 2025 April 25; revised 2025 November 16; accepted 2025 December 6; published 2026 January 20

Abstract

The upcoming 10 m class large Indian telescope is proposed to be built using segmented mirror technology. To achieve diffraction-limited image quality with a segmented mirror telescope, it is important to phase mirror segments with very high precision. We have explored an optical transfer function (OTF)–based technique for segment phasing. The major advantage of this approach is that it enables highly accurate phase measurements over a large capture range without requiring dedicated complex optics or mechanisms. Through extensive simulations and laboratory experiments, we have tested the feasibility of using this technique for the proposed large telescope. From extensive simulations, we found that by using optical filters of different bandwidths, the modulation transfer function allows a measurement of piston errors as large as 50–100 μm and can reduce this down to 25–30 nm. Another advantage of using the OTF is that it inherently allows simultaneous measurement of phase errors in a large number of mirror segments without the use of any specialized optical elements. In this paper we present our results from simulations and laboratory experiments in relation to the proposed 10 m class segmented mirror telescope.

Unified Astronomy Thesaurus concepts: Optical telescopes (1174); Astronomical instrumentation (799); Astronomical optics (88)

1. Introduction

In the era of giant telescopes with 30–40 m size primary mirrors, segmented mirror technology has become the preferred option, where a large primary mirror is formed by combining multiple smaller mirror segments. In order to achieve diffraction-limited performance with a segmented mirror telescope, the individual mirror segments must be aligned very precisely to follow the profile of the parent primary mirror. The alignment of segments involves three tasks: coalignment, cofocusing, and cophasing. Coalignment deals with the removal of segment tip-tilt errors, which is done by stacking up all the segment images together on a single point on the focal plane, and cofocusing is linked with removing the segment defocus error, which primarily arises due to a mismatch in the segment radius of curvature (ROC). However, cophasing of segments deals with the removal of segment piston errors. This process requires a specialized optical instrument, called the alignment and phasing system (APS). The APS may use any of the available wavefront sensing techniques to measure segment alignment errors. Once the segment positions are defined by the APS, the primary mirror control system (M1CS) maintains these segment positions over time, under varying external conditions.

The tasks of coalignment and cofocusing are usually performed by a device based on the principle of the Shack–Hartmann wavefront sensor. However, piston measurement is a rather challenging task, and hence various phasing techniques working in the physical optics domain are being developed. The presence of piston errors introduces phase errors in the wavefront, due to which the light from the individual segments adds up incoherently at the focal plane, consequently limiting the spatial resolution of the large segmented mirror telescope. Therefore, to attain spatial resolution and sensitivity equivalent to the full-size primary mirror, it is important to phase the segments in the order of a few nanometers.

Depending on the technique used, phase recovery can be made directly in the image plane, pupil plane, or intermediate plane. Most of the existing phasing techniques have a strong trade-off between their measurement range and accuracy. Hence these techniques are usually classified as coarse (large measurement range, low accuracy) and fine (measurement range $<\lambda/4$, high accuracy) phasing techniques. Therefore, to phase any segmented mirror telescope, one may have to use two different techniques for coarse and fine phasing. This makes the phasing instrument complex and the process time-consuming. Although many segmented mirror telescopes have been developed, the only telescopes on which phasing is performed regularly are the twin Keck telescopes (G. A. Chanan et al. 2000b). The pioneering broadband and narrowband phasing techniques developed for the Keck telescopes can phase their mirror segments with an rms accuracy of 30 nm and 6 nm, respectively (G. Chanan et al. 1998, 2000a). The dispersed fringe sensor (DFS; F. Shi et al. 2004) is another promising phasing technique that has been successfully used on the JWST for coarse piston measurements (D. S. Acton et al. 2022). However, recent developments have shown that DFS can also be used for fine phasing to measure piston errors smaller than $\lambda/4$ (Y. Li et al. 2017; Y. Li & S. Wang 2022; R. Dharmadhikari et al. 2023). Attempts have also been made to phase the mirror segments using phase discontinuity sensing (G. Chanan et al. 1999), interferometric technique (C. Pizarro et al. 2002), and the pyramid sensor (S. Esposito & N. Devaney 2002). Several other innovative

phasing techniques are currently under exploration (M. Troy et al. 2016, 2008, 2024; L. Li et al. 2023; M. Troy et al. 2024).

The use of the optical transfer function (OTF) for measuring segment tip-tilt and phase errors was introduced by F. Baron et al. (2008) and G. Guerri et al. (2010), where the phase component of the OTF was used to measure piston errors with a high accuracy of nearly 10 nm. However, this technique suffers from phase wrapping problems and can only measure piston errors $<\lambda/4$; thus it is found to be suitable only for fine phasing. Later, J. Jiang & W. Zhao (2016) and J. F. Simar et al. (2015) found that the secondary peak of the modulation transfer function (MTF) is strongly correlated with the piston error. Hence this property can be utilized to measure the segment piston error with an extended measurement range of up to 200 μm. Another important advantage of this technique is that we can simultaneously measure the piston errors from multiple intersegment regions without using any extra optical components. Through an extensive survey and after performing laboratory tests on various phasing techniques, we found the OTF-based phasing scheme to be most suitable for the proposed 10 m class Indian telescope.

A brief description of the proposed 10 m class Indian optical telescope and its alignment requirements are given in Section 2. The principle of OTF-based phasing scheme and related simulation results for are given in Section 3. Section 4 provides our experimental results in detail. The paper ends with a discussion and conclusion (Section 5).

2. The Indian Large Segmented Mirror Telescope

Over the past two decades, Indian astronomers have aspired to build a 10 m class telescope equipped with advanced instrumentation. In the late 1990s, the Indian Institute of Astrophysics (IIA) proposed a 6.5 m telescope. This led to site surveys in the trans-Himalayan region when Hanle in Ladakh (at 4500 m elevation) was identified as a suitable site for a large telescope. This resulted in the establishment of the Indian Astronomical Observatory (IAO), which currently hosts a 2 m class telescope. Subsequent characterization of the IAO site confirmed that it is a world-class site, equipped with all the necessary infrastructure required for a large observatory. One of the very important site-related parameters is atmospheric seeing and median seeing at IAO Hanle is found to be about 1″ (B. C. Bhatt et al. 2000; R. Cowsik et al. 2002). The proposed Indian large telescope is expected to be 8–14 m class and will be built using segmented mirror technology (G. C. Anupama et al. 2022). Currently the project is in its early planning and conceptualization phase. Several technology development projects have been initiated in the country to address the complexities of segmented mirror technology. As part of this effort, the criticalities linked with the phasing of primary mirror segments are investigated through simulations and laboratory experiments.

2.1. The Optomechanical Design

Many design options are proposed for the telescope; however, the preferred optical design is a Ritchey–Chrétien (RC). The effective size of the primary mirror is 11.6 m in diameter, made of 60 hexagonal segments of 1.4 m each. The telescope utilizes a standard alt-azimuth mount, and similar to the Keck telescopes, many options for the focal plane (such as Cassegrain, Nasmyth, and bent Cassegrain) have been envisaged. Figure 1 shows the three-dimensional model of the telescope. The RC optical design offers diffraction-limited image quality up to a 5′ (diameter) field of view; beyond this, the image performance degrades due to off-axis aberrations, like coma, astigmatism, and field curvature. The optical design parameters are given in Table 1, and the ZEMAX-generated optical layout is shown in Figure 1. The proposed first light instruments for this 10 m telescope include a seeing-limited,

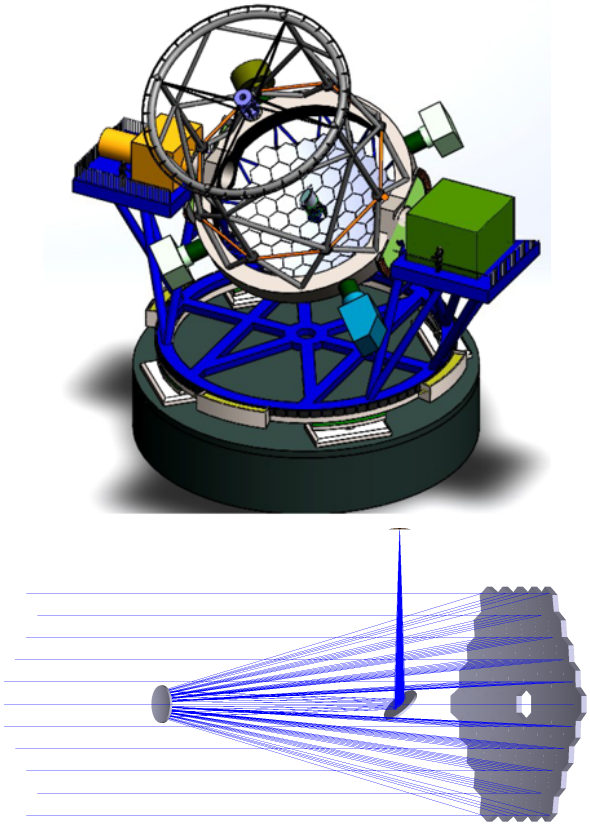

Figure 1. A three-dimensional model (top) and optical design layout (bottom) for India's proposed large segmented mirror telescope.

Table 1
Optical Design Details for India's Large Segmented Mirror Telescope

Parameter	Value
Primary Mirror	
ROC	35 m
F/#	1.5
Diameter	11.6 m
Conic constant	−1.00308462
Secondary Mirror	
ROC	4.57 m
Diameter	1.4 m
Conic constant	−1.66165862
Working F/#	12.5361
Effective focal length	145.409 m
Plate scale	1.4185"mm^{-1}
Primary secondary distance	15.49 m
Secondary tertiary distance	10.14 m
Back focal length	6.561 m
Focal plane ROC	2.053 m

Table 2
Alignment Requirements of the 10 m Class Segmented Mirror Telescope

Alignment Error	Seeing-limited Mode	Diffraction-limited Mode
Coaligning/tip-tilt error	$\leqslant$0.03"	$\leqslant$0.01"
Cofocusing/ROC error	$\leqslant$150 μm	$\leqslant$150 μm
Cophasing/piston error	$\leqslant$25–30 μm	$\leqslant$30 nm

0.3–1 μm low- to medium-resolution multiobject spectrometer camera; a 0.9–5 μm spectrometer camera; and a high-resolution ($R \approx$ 50,000–120,000) spectrometer in the 0.3–1 μm range (G. C. Anupama et al. 2022).

2.2. Alignment and Phasing Requirements

Allocating the error budget for segment alignment is crucial, as it decides the final telescope image quality. For the 10 m class segmented mirror telescope, we have attempted to come up with the requirements by using simulations as well as by referring to the practically achieved values in existing segmented mirror telescopes such as the Keck telescopes, Hobby-Eberly Telescope (HET), and the Southern African Large Telescope (SALT; G. A. Chanan et al. 1986; M. J. Wolf et al. 2003; A. Wirth et al. 2004). We have also used a Python ZEMAX interfacing-based tool to find alignment requirements for India's large segmented mirror telescope. The variation of image-quality parameters such as the D50, D80, and Strehl ratio is studied with varying alignment errors. These values are then used to define the alignment accuracy required for tip-tilt, defocus, and piston errors for seeing-limited and diffraction-limited imaging. The derived values are tabulated in Table 2. Considering that the initial segment piston error will be very large, the phasing scheme is expected to work over a large capture range of 50–100 μm, and at the same time it should have extremely precise measurement. The primary mirror is made of a large number of segments; hence, to reduce the telescope overhead, the phasing scheme should also facilitate simultaneous measurement of all the segment piston errors. Once the alignment requirements are defined, we proceed to test the feasibility of the OTF-based phasing scheme.

3. OTF-based Phasing: The Principle and Simulations

A schematic of an OTF-based phasing scheme for a segmented mirror telescope is shown in Figure 2. The light from a point source, such as a star, is reimaged after the telescope focal plane using a collimator and camera lens. A broadband filter and a mask are placed in the collimated beam. The sampled light is focused on the detector plane to get the point-spread function (PSF). In order to measure the segment tip-tilt and piston errors using the OTF, the light must be sampled from a pair of subaperture masks, as shown in the Figure 2. Without steering optics such as prism/lenslet, the OTF allows simultaneous measurement of piston errors from multiple segments (L. Zhang et al. 2023).

In the case of two mirror segments, the PSF observed on the detector plane (u,v) is a fringe pattern and is given by Equation (1). The complete derivation for Equation (1) can be found in J. Jiang & W. Zhao (2016):

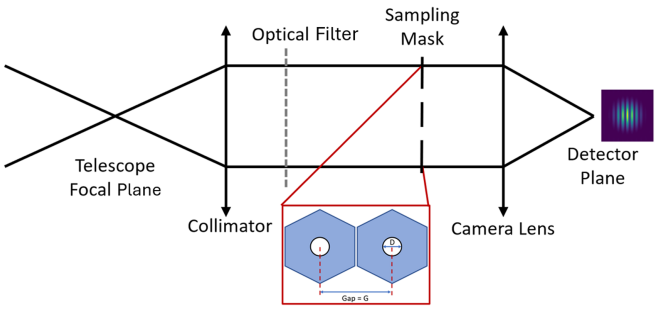

Figure 2. Optical layout for OTF-based tip-tilt and piston measurements. Inset: the sampling aperture mask.

$$\mathrm{PSF}(u,\ v,\ \lambda) = \frac{D^3 {J_1}^2 \pi}{\sqrt{u^2 + v^2}} \left[1 + \cos 2\pi \left(\frac{p}{\lambda} - uG\right)\right], \quad (1)$$

where p is the piston error, D is the sampling aperture diameter, G is the gap between the subapertures, J_1 is the first-order Bessel function, $u = x/(\lambda f)$, and $v = y/(\lambda f)$, with f being the focal length of the camera lens. Equation (1) contains two terms: the first corresponds to the diffraction term, and the second is the interference term. From Equation (1) we see that the piston value p affects the interference term. In the next step, this PSF is Fourier transformed to get the OTF. The OTF is a complex quantity that consists of real and imaginary parts. The magnitude of the OTF forms the MTF, whereas the phase term forms the phase transfer function (PTF). Both of these terms contain information about the tip-tilt and piston errors of the mirror segments.

3.1. Phasing with the PTF

The use of the OTF for phasing in a segmented mirror telescope was first introduced by F. Baron et al. (2008), where the phase part of the OTF (the PTF) was utilized for piston measurements. It was noticed that for very small values of piston errors, the MTF almost remained invariant, whereas the PTF showed a strong dependence on the piston error. The PTF is obtained as the phase component of the OTF; hence it gives the wavefront phase map of the sampled apertures. This wavefront phase map can be used to derive the complete wavefront aberrations, including the segment tip-tilt, piston, and defocus errors. However, in this study, we focus only on piston measurements. The measured wavefront phase map has a cyclicity of π in terms of phase, which translates to a cyclicity of $\pm\lambda/4$ in terms of piston error (see Figure 3). Hence the measurement range of the PTF-based technique is limited to $\pm\lambda/4$ piston errors. Thus it can only be used for fine phasing of mirror segments.

3.2. Phasing with the MTF

The PTF-based piston measurement has a limited range of $\pm\lambda/4$; however, the MTF, which is the magnitude component of the OTF, can also be used for piston measurements. The MTF is also known as the contrast transfer function, and blurring of the PSF in the presence of piston errors directly affects the MTF. If we consider two segment subapertures with piston errors, then the simulated PSF and corresponding MTF subjected to varying piston errors are shown in Figure 4.

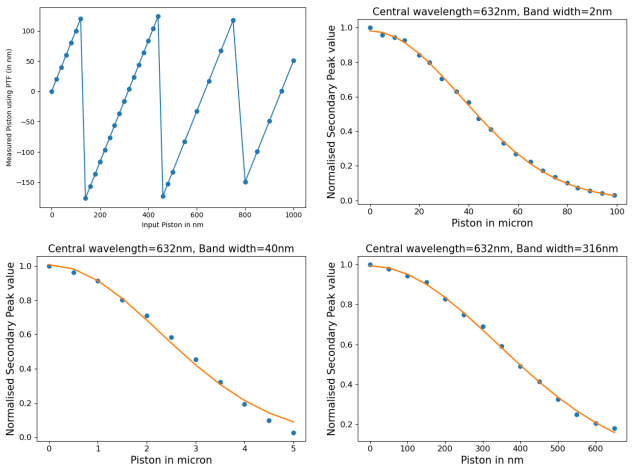

Figure 3. Simulation showing the cyclic variation of the PTF-based piston errors (top left). Plots showing variation of normalized secondary peak values of the MTF against piston errors, under ideal conditions for different bandpass filters.

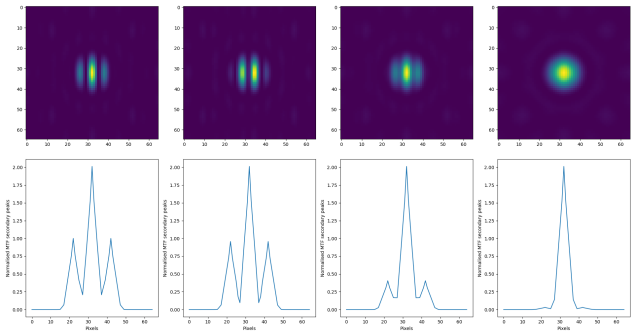

Figure 4. Simulated PSF for piston errors of 0, 10, 50, and 100 μm, respectively (top panel). Normalized intensity plots of the corresponding MTF, showing the diminishing secondary peak (bottom panel).

The cross-sectional plot of the MTF has one central peak and two secondary peaks (bottom panel in Figure 4). From the figure, it is clear that the intensity of the central main peak remains unaffected by the piston errors, whereas the intensity of the secondary peaks reduces as the piston error increases. The intensity of the secondary peak is maximum for zero piston error; therefore, it is used to normalize the MTF. The variation of the normalized secondary peak intensity value against the piston error is shown in Figure 3. The normalized secondary peak value reduces with increasing piston error and follows a Gaussian trend. The measurement range of this technique is limited to the coherence length of the filter ($\lambda^2/2\Delta\lambda$). For piston errors larger than the coherence length, the PSF becomes completely blurred, and the normalized secondary peak value of the MTF becomes close to zero. This sets the upper limit for the piston measurement range. By using different filters with varying coherence lengths, the piston measurement range and accuracy can be varied. Figure 3 shows the variation of the MTF secondary peak values with piston errors for three different filters with a central wavelength of 632 nm and bandwidths of 2, 40, and 316 nm. For each case, the coherence length (which is equal to the measurement range) is 100 μm, 5 μm, and 632 nm, respectively. In principle, by using a very wide bandpass filter, the MTF itself can be used to measure small piston errors ($<\lambda$). However, the PTF shows a strong dependence on the segment piston error and hence can precisely measure small phase errors (F. Baron et al. 2008; G. Guerri et al. 2010). So, by using magnitude and phase parts of the same OTF, one can precisely measure piston errors, starting from a few nanometers to hundreds of microns.

3.3. Simulations for Phase Measurements

Ideally, the OTF scheme can be used for segment phasing for coarse and fine piston error measurements; however, under practical conditions, several external factors may affect the measurement accuracy. Therefore, it is important to understand the effects of external parameters on the performance of OTF-based phasing. We have developed a Python-based simulation code that includes different factors which affect the phase measurements, such as the stellar magnitude, atmospheric turbulence and extinction, sky and moon background, transmissivity losses, detector noises, etc. The simulation code can generate a PSF for any given telescope + APS. Using this simulation code, we have attempted to explore the effects of stellar magnitude, exposure time, atmospheric seeing, sampling aperture size, baseline, and orientation on OTF-based phasing results.

3.3.1. Atmospheric Seeing, Aperture, and Stellar Brightness

In the presence of atmospheric turbulence, the measured wavefront phase is not only subjected to segment piston errors but also includes atmospheric aberrations, which may have adverse effects on piston measurement accuracy. To understand the effect of atmospheric turbulence on MTF-based piston measurements, we first used a relatively bright star with short exposure (5 ms) and small subaperture (with a gap of 20 cm). We found that secondary peak values are strongly affected by atmospheric seeing, and hence the conventional method of normalization, in which the value of the secondary peak of any measured piston error is divided by the peak value of the zero piston error, does not work. This is because the maximum value of the secondary peak changes with varying atmospheric conditions, thus requiring a separate normalization factor for each pair of segments, which is practically impossible to measure. To resolve this issue, instead of normalizing the maximum intensity of the MTF secondary peak, we normalized the total flux associated with the secondary envelope. The flux is obtained by summing the total intensity values within the secondary peak region, as shown in Figure 5.

By making use of different filters and varying atmospheric seeing (0.8"–1.5"), we could very well manage to recover the phase errors injected between two neighboring mirror segments (see Figure 6). Here the piston errors have been derived using a mean of five simulated data points with random phase screens generated for each case. For each exposure, to incorporate the wind effect, the phase screen is dynamically moved (and the wind speed considered is 10 m s^{-1}). The real-time phasing of a segmented mirror telescope is possible only when one would make use of faint stars. However, to achieve the required signal-to-noise ratio (SNR) with a faint star, the exposure time, aperture diameter, or both need(s) to be increased. An increased exposure time leads to blurring of the PSF due to image motion and hence strongly affects the MTF-based phase recovery. Similarly, increasing the subaperture size also resulted in precision loss,

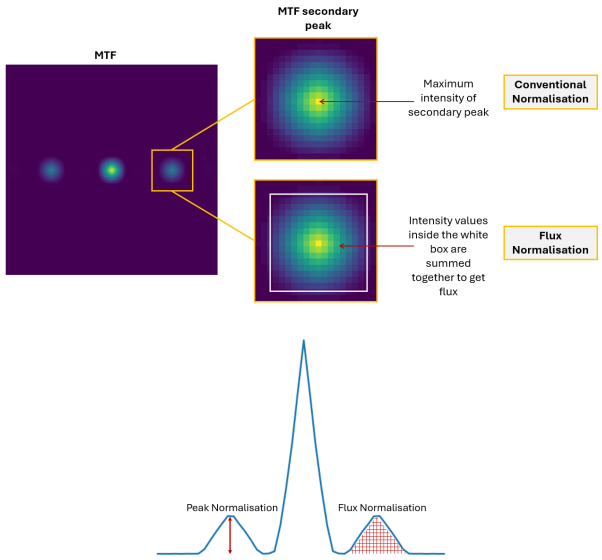

Figure 5. Working of conventional peak versus flux normalization of the MTF. Note the two-dimensional image of the MTF (top) and corresponding intensity plot showing values used for peak and flux normalization in red color (bottom).

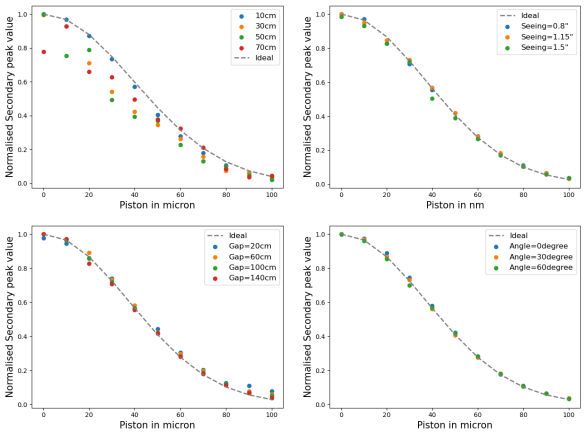

Figure 6. Variation of flux normalized MTF secondary peak values with input piston errors for varying aperture diameters (top left), atmospheric seeing (top right), varying gap (bottom left), and varying orientation (bottom right).

most likely due to the presence of the speckles, which in turn degrade the PSF as well as the MTF (see Figure 6). Hereafter, to attain the best possible piston measurement accuracy, we have used a bright star, short exposure, and small sampling aperture size comparable to the Fried parameter r_o.

In order to measure piston error $<\lambda/4$, when we attempted to make use of the PTF-based fine phasing, we found it to work very well for a single pair, as well as for simultaneous measurement of piston errors of multisegments. However, in the presence of atmospheric seeing, contrary to the MTF, the PTF-based phasing seems to work only with the long exposure and the shorter baseline between two subapertures. The latter limitation makes it unsuitable for the simultaneous piston measurement of a large number of mirror segments.

3.4. Phasing Multiple Mirror Segments Simultaneously

The simulation results presented in the previous section consider only one pair of segments. However, in practice we need to measure the piston errors of all segments simultaneously. To achieve this, the phasing device of the Keck telescopes uses a set of prisms to separate light from different intersegment regions on the detector plane, thus increasing the number of components. In contrast, by using a suitable mask, the OTF-based phasing scheme inherently provides the capability to measure multiple segments simultaneously without requiring any extra optics in the phasing device. For any segmented primary mirror, the gaps between two subapertures and their orientation would vary by a large amount. Therefore, before initiating simulation studies on multiple segments, we first explored the effect of increasing the baseline and the change of orientation of the two subapertures on MTF-based measurements. It was found that under short exposure with a bright star, the increasing gap and changing orientation angle has negligible effects (see Figure 6). One of the challenging tasks related to the simultaneous measurement is designing the aperture mask, so that the secondary peaks of the MTF would not overlap. Since the gap between two subapertures and their orientation decides the spatial position of the secondary peaks of the MTF, the configuration of subapertures should be chosen such that their secondary peaks do not overlap. L. Zhang et al. (2023) have developed an algorithm to define the mask positions so that overlapping is avoided. The proposed method works well up to 18 segments, beyond which it becomes difficult to avoid overlapping, and one needs to make use of more than one set of masks. The 10 m Indian telescope will have 60 segments, comprising 6 sectors with 15 segments each. Therefore, we propose to phase the primary mirror sector-wise. Figure 7 shows a single sector with 15 segments and the optimized position of the corresponding subaperture masks. For our simulations, the segment number 0 is considered as the reference and all piston measurements are carried out with respect to this segment. The MTF image for the corresponding aperture geometry is also shown in Figure 7, on which the secondary peaks formed by each segment via pairing with the 0th segment are marked with red stars.

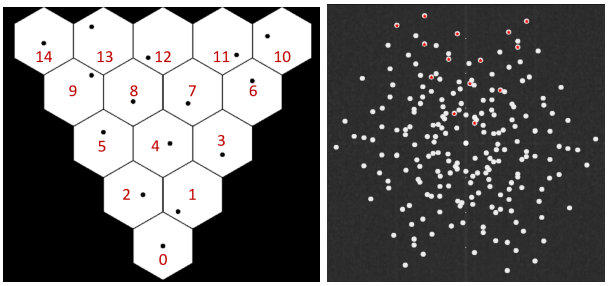

Figure 7. Multisegment piston measurements for one sector. Placement of subapertures (the black circles) indicate the position of the 10 cm size apertures on each segment (left). Corresponding MTF: the red stars indicate the MTF secondary peaks for each of the marked segments formed with respect to the reference segment.

The simulations for sector-wise piston measurements are initially conducted without considering the atmosphere. Following the successful simultaneous measurement of piston errors across the entire sector, we then introduced atmospheric seeing. The variable piston errors are injected into different segments, and a single MTF image (similar to one shown in Figure 7) is used to derive the piston values of individual segments. The mean value of the measured piston for the 14 segments is plotted against the input piston for different filters, as shown in Figure 8. The rms error of the fitting is considered

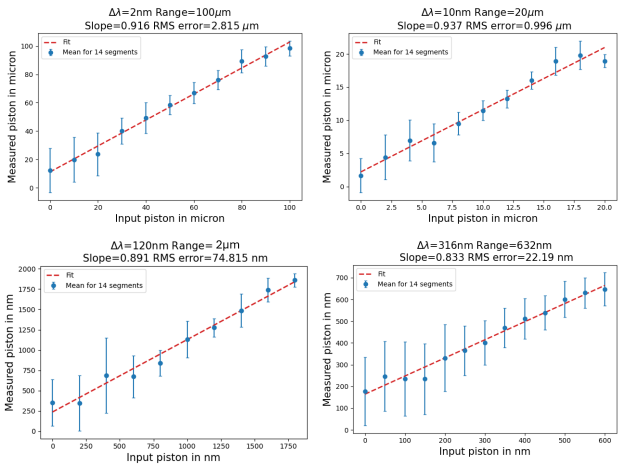

Figure 8. Multisegment piston measurements for one sector: plots showing applied versus mean of measured piston values for 14 segments using various filters.

as a measure of the accuracy. The mean value of the slope and rms error derived using 14 segments for different filters are given in Table 3. From the simulation results given in this table, it is quite clear that by making use of a set of suitable filters and masks, one can precisely measure piston errors over a very wide capture range with high precision. By making use of a broadband filter, we achieved a piston measurement accuracy of 25–30 nm with the MTF; this eliminates the need of using the PTF for fine phasing.

4. Experimental Validation of OTF-based Phasing

4.1. Laboratory Setup

Our simulations show that the OTF can be a preferable choice for phasing mirror segments of the proposed large telescope. However, testing and validating these simulation results through laboratory experiments is important. The laboratory setup for the OTF-based experiment is shown in Figure 9. As shown in Figure 3, the measurement range of MTF-based piston measurement depends on the coherence length of the light source; hence we use a broadband light source with different filters and a laser source. An achromatic doublet lens is used to generate a collimated beam of 50 mm diameter, which is reflected toward two plane mirror segments using beam splitter 1. The mirrors are mounted on a high-precision linear actuator from Thorlabs, which allows precise movement of the mirror segment along the optical axis, thus helping introduce any desired piston error. The reflected light from the mirror segments returns to beam splitter 1 and is transmitted further toward a second beam splitter that splits the beam into two perpendicular arms. The light reflected from beam splitter 2 is used for performing OTF-based phasing (shown with a blue dotted line in Figure 9), whereas the transmitted light is used for DFS-based phasing measurements (shown with a red dotted line in Figure 9). In the OTF arm, we have an aperture mask that samples light from both segments through two circular regions of 6 mm diameter each. This light is then focused onto the detector plane of the complementary metal-oxide-semiconductor detector using a camera lens. The recorded image of the PSF is then Fourier transformed to obtain the OTF, and then the MTF/PTF can be used to derive the piston values. The specification of the components used in

Table 3
Simulation Results for MTF-based Piston Measurements for One Sector

Filter Bandwidth	Measurement Range	Slope for Mean of 14 Segments	rms Error for Mean of 14 Segments
2 nm	100 μm	0.91	2.81 μm
10 nm	19.97 μm	0.93	0.99 μm
120 nm	1.76 μm	0.89	74.81 nm
316 nm (20 runs)	632 nm	0.83	22.19 nm

the experiment is given in Table 4. We have used a laser source of 2 nm bandwidth to provide the largest capture range ($\sim$100 μm). Further, to reduce the measurement range and improve the measurement accuracy, we use two different filters along with a broadband tungsten light source. A filter with a 10 nm bandwidth and 650 nm central wavelength provides a measurement range of 20 μm. In contrast, the Johnson–Bessel *R* filter, with a central wavelength of 630 nm and bandwidth of 120 nm, provides the most accurate piston values over a very small range ($\sim$1.65 μm). Multiple sets of experiments are performed with a laser and two filters, and the results of these phasing experiments are discussed in the subsequent section. Spectral specification of the laser, the two filters, and their measurement range are given in Table 4.

4.2. Experimentation-related Results

4.2.1. Piston Measurements with the MTF

Before performing the experiment, it is important to calibrate the variation of MTF secondary peak values against piston errors for each filter. Different methods can be adopted to convert the experimentally obtained MTF secondary peak values into piston errors. The most commonly used method is to use a Gaussian function derived from simulations (provided the wavelength-dependent throughput functions for all components are known precisely). Another more accurate method is to use an experimental calibration, where we obtain the relation by fitting a higher-order polynomial to the normalized MTF secondary peaks obtained experimentally. We have tested with both the calibration schemes and finally used the polynomial fitting.

For normalization, the secondary peak values of the MTF must be known precisely at zero piston error. To ascertain that mirror segments are at zero piston position, we have included the DFS phasing scheme in the same experimental setup (with the DFS arm shown in red in Figure 9). At zero piston condition, the DFS fringes disappear entirely, giving rise to a continuous source spectrum. Before every OTF run, the DFS is used to ensure the zero piston condition, and then a known piston error is applied by moving one of the mirror segments. The experiment is conducted for three cases: (i) laser, (ii) narrowband filter, and (iii) broadband Johnson–Bessel *R* filter. While conducting the experiment for MTF-based measurements, a linear actuator is used to move one of the mirror segments with a step size of 1 μm, 500 nm, and 100 nm for the laser, narrow, and broadband filters, respectively. An external high-precision optical encoder system is also used to ensure that applied piston error is indeed executed. At each step, 30 PSF images are recorded and then these images are Fourier transformed to get the MTF. Figure 9 (bottom) shows an

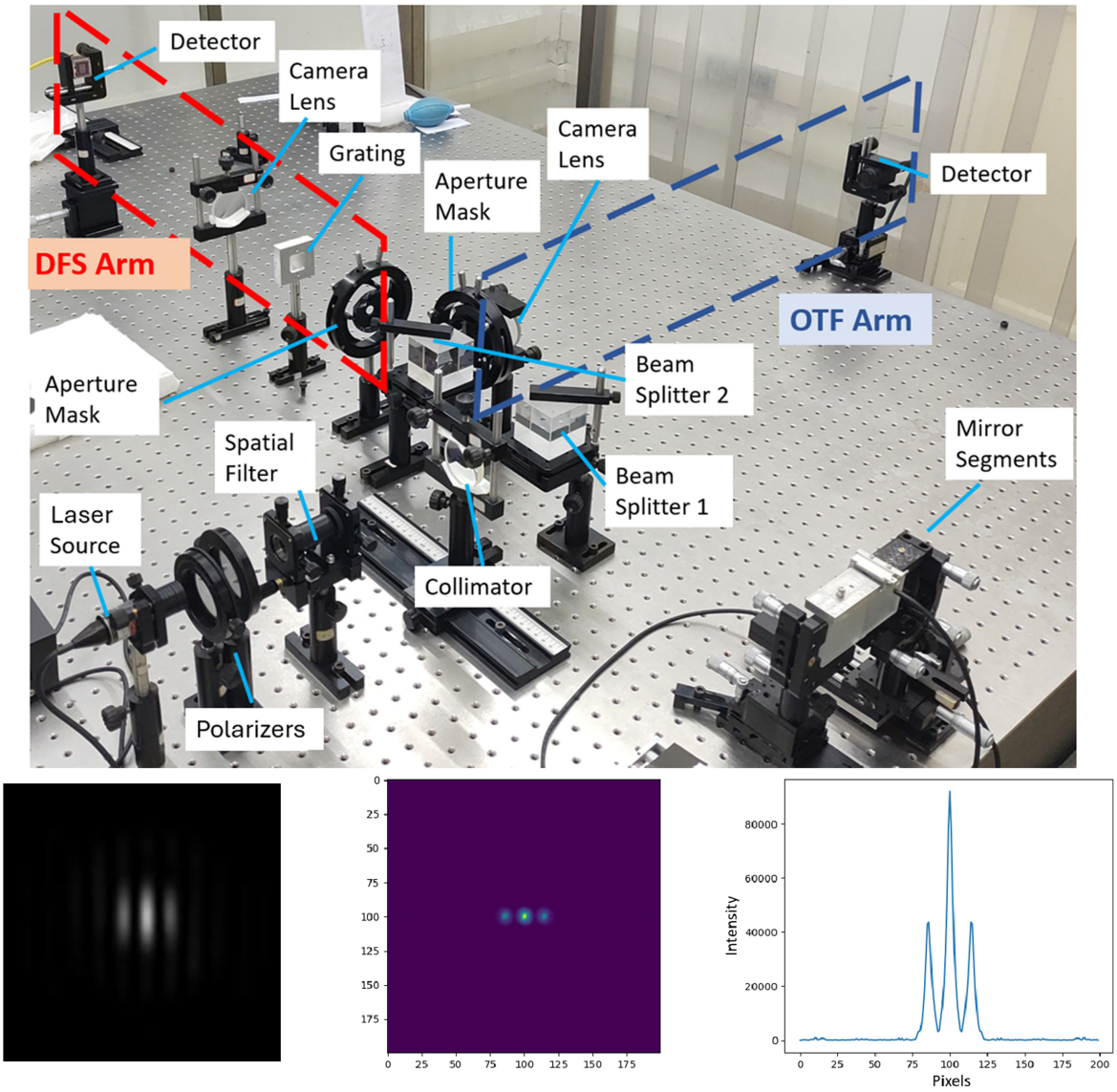

Figure 9. Laboratory experimentation setup for the OTF-based phasing experiment (top). Experimentally observed PSF (bottom left) and the corresponding MTF (bottom middle) and the intensity plot of the MTF (bottom right).

Table 4
Experimental Setup and Filter Details

Parameter	Value		
Source	Thorlabs Broadband Tungsten Lamp and laser (635 nm)		
Point source	10 μm pinhole		
Collimator lens	150 mm focal length achromatic doublet		
Mirror segments	$\lambda/8$ surface quality plane mirrors		
Sampling aperture	6 mm diameter, 12 mm gap		
Camera lens	750 mm focal length achromatic doublet		
Detector	3.45 μm pixel size		
Filter	Central Wavelength (λ)	Bandwidth ($\delta\lambda$)	Coherence Length ($\lambda^2/2\delta\lambda$)
Laser	632 nm	2 nm	100 μm
Narrowband	650 nm	10 nm	21.25 μm
Johnson–Bessel R	630 nm	120 nm	1.653 μm

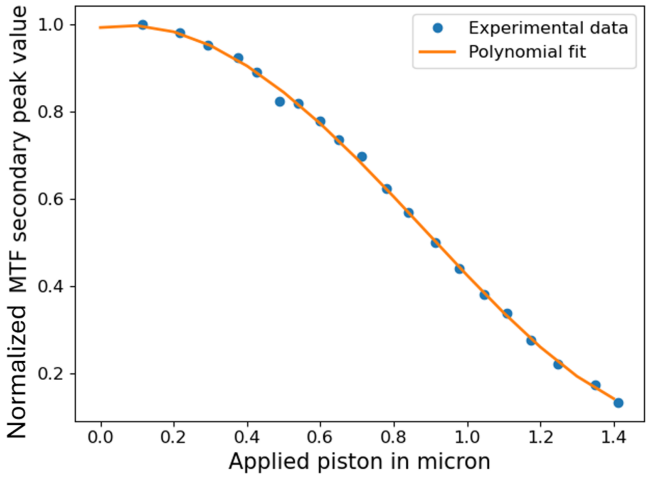

Figure 10. Variation of normalized MTF secondary peaks with applied piston values for experimental data for the broadband Johnson–Bessel R filter and corresponding polynomial fit used for calibration.

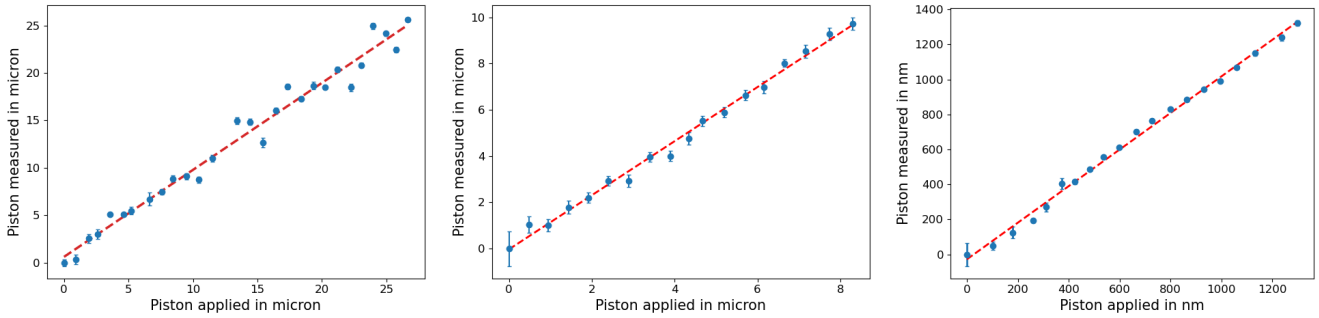

Figure 11. Plot showing experimentally measured piston values versus applied piston values with laser source (left), narrowband filter (middle), and Johnson–Bessel *R* filter (right).

Table 5
Experimental Results for the OTF-based Phasing for Piston Measurements Obtained Using the MTF (Top) and the PTF (with the Johnson–Bessel *R* Filter; Bottom)

Filter Used	Measurement Range	Fit Slope	rms Error
Laser	100 μm	0.9	700 nm
Narrowband	20 μm	1.17	328 nm
Johnson–Bessel *R*	1.6 μm	1.096	35.145 nm
Experiment dataset number	**Cycle number**	**rms error**	**Mean rms error**
Set 1	Cycle 1	1.724 nm	1.651 nm
	Cycle 2	1.514 nm	
	Cycle 3	1.303 nm	
	Cycle 4	0.864 nm	
Set 2	Cycle 1	2.227 nm	6.061 nm
	Cycle 2	12.584 nm	
	Cycle 3	3.373 nm	
Set 3	Cycle 1	1.669 nm	1.047 nm
	Cycle 2	1.141 nm	
	Cycle 3	1.282 nm	
	Cycle 4	0.247 nm	
	Cycle 5	0.275 nm	
	Cycle 6	1.670 nm	

example of the experimentally recorded PSF image and the corresponding MTF obtained with the laser source. The value of the MTF secondary peak of every set is normalized with respect to the secondary peak of the zero piston. Then the calibration curve is used to convert the normalized value of the secondary peaks into corresponding piston values. Figure 10 shows an example of the normalized MTF secondary peak variation against the applied piston values for the narrowband filter. To have precise piston measurements, we fit a fourth-order polynomial on the MTF data. Then the applied versus measured piston values are plotted, and a straight line is fitted onto the data (Figure 11). Ideally, the slope of this straight line should be one; the experimentally obtained slope values for each of these cases are tabulated in Table 5. Considering that the external optical encoder reads the applied piston error precisely, the scatter around the straight line can be attributed to the accuracy of the piston measurement. Table 5 gives the rms values for each case. To ensure the repeatability of the experiment, the experiment was conducted multiple times; hence the values given in Table 5 are the mean values of slope and rms errors. From Table 5, it is clear that the measurement

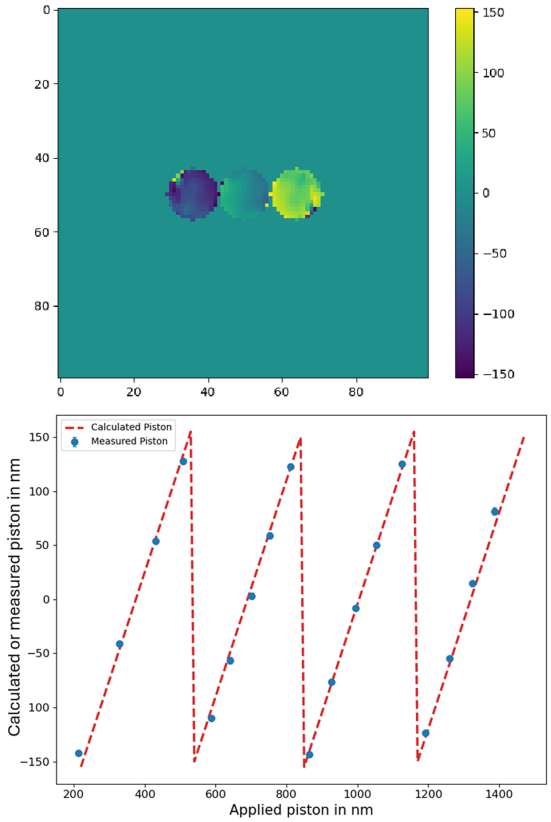

Figure 12. An example of the wavefront phase map (PTF) obtained from experimental data (top). Experimental data showing the plot for applied versus measured piston values (bottom). The red dotted lines indicate the calculated piston values.

accuracy improves with the increasing bandwidth (and reducing measurement range) of the filter. Thus the results confirm that by using different filters, very precise measurement of the segment piston error over a wide range using the MTF alone is possible.

4.2.2. Piston Measurements with the PTF

Using the broadest bandwidth filter, the best MTF-based piston measurement accuracy achieved in our laboratory experiment is about 35 nm. However, simulations show that under atmosphere-free conditions, the PTF can be used to narrow down this accuracy value to a few nanometers; hence to verify this experimentally we now use the PTF to measure piston values. Figure 12 shows an example PTF (phase map)

extracted from the same observation as used for the MTF with the broadest filter of 120 nm bandwidth. The phase map consists of three circular regions. The central region corresponds to zero phase, whereas the two side regions correspond to the phase maps, which are complex conjugates of each other. The wavefront phase map is obtained by taking data from any one of the circular regions on the side. Then the average phase value is directly derived from the phase map. Further, the phase is converted to piston by multiplying with $\lambda/4\pi$. The measured piston values are plotted against the applied piston values as shown in Figure 12, where one can observe the effect of π phase wrapping (cyclic behavior). Each cycle of the measured piston data is fitted with a separate straight line, and the rms error derived from the fitting denotes the precision of the measurements. To ensure the robustness of the PTF measurement, we have conducted three runs, distributed over many days/weeks, and each set of data covers multiple cycles. The rms values of each cycle and the average value of a particular dataset are given in Table 5. Previously, G. Guerri et al. (2010) and F. Baron et al. (2008) have reported a piston measurement accuracy of ≈11 nm using the PTF, whereas in our experiments we achieved a piston measurement accuracy in the range of 0.25–12.6 nm.

5. Discussion and Conclusion

The cophasing of segmented mirrors is one of the most challenging tasks, and several phasing schemes are being developed to improve the phasing accuracy and reduce system complexities. Among all these diverse schemes, the OTF-based segment phasing approach appears very promising. The major advantage of this scheme is that without the use of dedicated complex optics and mechanisms, it can facilitate very accurate phase measurements over a very large capture range. In this scheme, the magnitude and the phase part of the OTF are used to derive segment piston errors. In order to check the feasibility of implementing this phasing scheme on India's large proposed segmented mirror telescope, we have carried out extensive simulations and laboratory experimentation.

We have utilized our Python-based end-to-end simulation code to predict the performance of MTF- and PTF-based coarse and fine measurements under varying external conditions. The measurement range of the MTF is limited to the coherence length of the filter used ($\lambda^2/2\Delta\lambda$). However, by following the method utilized in the Keck broadband phasing scheme, using a set of optical filters with varying coherence lengths, the piston measurement range and accuracy of the MTF method can be varied. Assuming that at the time of installation of mirror segments, these segments can be subjected to piston errors in the range of a few tens of microns, a filter with a fairly large coherence length can be used to measure these initial large piston errors. Subsequently, by using filters with larger bandwidths and, conversely, reduced coherence length, piston errors can be brought down to a few nanometers. Our simulation shows that a bright star of 5th magnitude with an exposure time of a few milliseconds can provide the desired measurement accuracy with the MTF. From the simulations, we have demonstrated that considering all external factors, the MTF can measure segment piston error with an accuracy of a few nanometers (<30 nm). The OTF-based phasing simulations are also presented by F. Baron et al. (2008), J. Jiang & W. Zhao (2016), and W. Zhao & Q. Zeng (2017), where they have achieved a better phasing accuracy; however, our simulation incorporates multisegment measurements in the presence of atmospheric turbulence and other noises, which affects the achievable phasing accuracy. For fine phasing, we found that PTF-based measurements are strongly affected by atmospheric effects, and hence in presence of atmosphere, we need to use the MTF with a very broad bandpass filter for fine phasing. Although the use of the PTF for ground-based telescopes is limited by atmosphere, it can be a potential candidate for a space-based telescope. The simple optical design and capability to sample multiple segments simultaneously makes OTF-based phasing a possible candidate for future space-based telescopes, such as the Habitable Worlds Observatory.

In order to verify the simulation findings on the OTF-based phasing scheme, we have also conducted extensive laboratory experiments. Once an image of the PSF subjected to two mirror segments is grabbed, then both the MTF and the PTF are derived through image analysis. When the piston error is larger than $\pm\lambda/4$, the MTF is best suited for deriving the piston error; otherwise, the PTF provides fine phase measurements. In the coarse phasing experiment with the MTF, we used three different filters, covering a wide range of piston errors. With the MTF, we could measure piston error as large as 40–50 μm using a laser source of about 2 nm bandwidth. Comparatively, through the widest broadband Johnson–Bessel R filter, a piston measurement accuracy of 35 nm has been achieved. Previously, J. F. Simar et al. (2016) and J. Jiang & W. Zhao (2016) have reported a measurement accuracy ≈16 nm with the MTF, which is slightly better than ours. In a large telescope, by making use of adaptive optics, diffraction-limited imaging is usually accomplished in near-infrared (NIR) wavelength bands. Therefore, segments phased with 30–50 nm rms accuracy would be good enough to provide acceptable image quality in the NIR, as is done using broadband phasing in the Keck telescopes. Therefore, we believe that by making use of a very wide bandpass optical filter, the MTF itself can measure the piston error to the required accuracy, which will make the telescope diffraction limited in the NIR wavelength bands (G. Chanan et al. 1998; G. Chanan & M. Troy 2018). The Johnson–Bessel R filter, which has the smallest measurement range in the MTF mode, is also used in the PTF experiment. We have conducted multiple experiments spanning several days and have achieved a piston measurement accuracy in the range of sub-nanometer to about 12 nm. Our experimental piston measurement accuracy using the PTF is better than the one obtained by G. Guerri et al. (2010) and F. Baron et al. (2008). However, it is in agreement with many other high-precision phase measurements reported using diverse techniques (C. Pizarro et al. 2002; F. Gonté et al. 2009; I. Surdej et al. 2010; M. Deprez et al. 2018; Y. Li & S. Wang 2022; L. Li et al. 2023). We believe that by using a larger bandwidth filter and improving the experimental setup, measurement accuracy can be further improved for both MTF- and PTF-based measurements. The PTF-based phasing performs exceptionally well both in laboratory settings and in simulations without an atmosphere. However, simulation-based studies carried out in the presence of atmospheric turbulence impose difficulties for recovering the piston errors consistently and precisely. Even with excellent seeing, the dynamic phase error introduced by the atmosphere is expected to be quite large (a small fraction of the wavelength), and it does not get completely nullified,

even for long exposures. Further study on the use of the PTF for fine phasing in the presence of atmosphere is required.

Without requiring any additional optics, by just making use of an optimized mask, the OTF-based phasing scheme also facilitates the simultaneous measurement of piston errors in a large number of mirror segments. We could manage to create a mask that can be used for simultaneous piston measurement of a whole sector comprising 15 mirror segments. However, we believe that by using a smart algorithm, it is quite possible to design a suitable mask that can even measure piston errors of more than a sector. Since the proposed 10 m class telescope is expected to have about 60 segments, we may have to use 2–3 sets of interchangeable masks. In case we succeed to accommodate 30 or more segments with a single mask, then we could cover all 60 segments with two masks, and there is a possibility to split the input beam into two parts for each mask. This would allow simultaneous measurement of the piston errors of all 60 segments. Another important aspect of the use of the MTF with a set of broadband filters is that, unlike with the Keck broadband phasing scheme, it does not require one to perturb the phasing state of the mirror segments. Despite these advantages, one of the caveats that remains unresolved is that MTF-based piston measurements are symmetric for positive and negative piston values; thus the sign ambiguity may not be resolved with MTF-based measurements alone. Further exploration is required to develop a smart technique/algorithm that can provide the exact piston state of all segments with an optimum number of iterations.

After exploring many different phasing techniques, we find the OTF-based phasing scheme most suitable for the proposed Indian large telescope. In the coming years, we intend to further explore this phasing scheme through simulation as well as experimentation.

Acknowledgments

We would like to thank the Indian Institute of Astrophysics (IIA) Mechanical Workshop team for helping with the design and fabrication of various customized mounts that are used in our phasing experiments. This research has made use of the high-performance computing (HPC) system of the Computer Center of the IIA, Bangalore.

ORCID iDs

Radhika Dharmadhikari https://orcid.org/0000-0003-0678-462X

References

Acton, D. S., Knight, S., Carrasquilla, M., et al. 2022, SPIE, 12180, 121800U
Anupama, G. C., Maheswar, G., Sriram, S., et al. 2022, JApA, 43, 32
Baron, F., Mocoeur, I., Cassaing, F., & Mugnier, L. M. 2008, JOSAA, 25, 1000
Bhatt, B. C., Prabhu, T. P., & Anupama, G. C. 2000, BASI, 28, 441
Chanan, G., Ohara, C., & Troy, M. 2000a, ApOpt, 39, 4706
Chanan, G., & Troy, M. 2018, SPIE, 10700, 107001E
Chanan, G., Troy, M., Dekens, F., et al. 1998, ApOpt, 37, 140
Chanan, G., Troy, M., & Sirko, E. 1999, ApOpt, 38, 704
Chanan, G. A., Nelson, J. E., & Mast, T. S. 1986, SPIE, 628, 466
Chanan, G. A., Troy, M., & Ohara, C. M. 2000b, SPIE, 4003, 188
Cowsik, R., Srinivasan, R., & Prabhu, T. P. 2002, BASI, 30, 105
Deprez, M., Wattellier, B., Bellanger, C., Lombard, L., & Primot, J. 2018, OExpr, 26, 5212
Dharmadhikari, R., Parihar, P., & Jacob, A. 2023, ExA, 56, 569
Esposito, S., & Devaney, N. 2002, ESOC, 58, 161
Gonté, F., Araujo, C., Bourtembourg, R., et al. 2009, Msngr, 136, 25
Guerri, G., Roose, S., Stockman, Y., et al. 2010, SPIE, 7731, 773154
Jiang, J., & Zhao, W. 2016, OExpr, 24, 19123
Li, L., Pan, A., Li, C., & Zhao, H. 2023, OptCo, 537, 129393
Li, Y., & Wang, S. 2022, OptLE, 159, 107187
Li, Y., Wang, S., & Rao, C. 2017, ApOpt, 56, 4267
Pizarro, C., Arasa, J., Laguarta, F., Tomas, N., & Pinto, A. 2002, ApOpt, 41, 4562
Shi, F., Chanan, G., Ohara, C., Troy, M., & Redding, D. C. 2004, ApOpt, 43, 4474
Simar, J. F., Stockman, Y., & Surdej, J. 2015, ApOpt, 54, 1118
Simar, J. F., Stockman, Y., & Surdej, J. 2016, SPIE, 9906, 99065F
Surdej, I., Yaitskova, N., & Gonte, F. 2010, ApOpt, 49, 4052
Troy, M., Bikkannavar, S., Kee, A. G., et al. 2024, SPIE, 13092, 130925R
Troy, M., Chanan, G., Michaels, S., et al. 2008, SPIE, 7012, 70120Y
Troy, M., Chanan, G., Michaels, S., et al. 2016, SPIE, 9906, 99066A
Wirth, A., Gonsiorowski, T., Roberts, J., et al. 2004, SPIE, 5489, 892
Wolf, M. J., Palunas, P., Booth, J. A., et al. 2003, SPIE, 5489, 714
Zhang, L., Zhao, W., Zhao, Y., Liu, J., & Chu, C. 2023, OptCo, 530, 129182
Zhao, W., & Zeng, Q. 2017, OExpr, 25, 24540